Adaptive Online Self-Gating (ADIOS) for Free-Breathing Noncontrast Renal MR Angiography

Yibin Xie[1,2], **Zhaoyang Fan**[2], **Rola Saouaf**[3], **Yutaka Natsuaki**[4], **Gerhard Laub**[4], and **Debiao Li**[1,2,*]

[1]University of California, Los Angeles, Department of Bioengineering, Los Angeles, California, USA

[2]Cedars-Sinai Medical Center, Biomedical Imaging Research Institute, Department of Biomedical Sciences, Los Angeles, California, USA

[3]Cedars-Sinai Medical Center, Department of Imaging, Los Angeles, California, USA

[4]Siemens Medical Solutions, Los Angeles, California, USA

Abstract

Purpose—To develop a respiratory self-gating method, adaptive online self-gating (ADIOS), for noncontrast MR angiography (NC MRA) of renal arteries to overcome some limitations of current free-breathing methods.

Methods—A NC MRA pulse sequence for online respiratory self-gating was developed based on three-dimensional balanced steady-state free precession (bSSFP) and slab-selective inversion-recovery. Motion information was derived directly from the slab being imaged for online gating. Scan efficiency was maintained by an automatic adaptive online algorithm. Qualitative and quantitative assessments of image quality were performed and results were compared with conventional diaphragm navigator (NAV).

Results—NC MRA imaging was successfully completed in all subjects (n=15). Similarly good image quality was observed in the proximal–middle renal arteries with ADIOS compared with NAV. Superior image quality was observed in the middle-distal renal arteries in the right kidneys with no NAV-induced artifacts. Maximal visible artery length was significantly longer with ADIOS versus NAV in the right kidneys. NAV setup was completely eliminated and scan time was significantly shorter with ADIOS on average compared with NAV.

Conclusion—The proposed ADIOS technique for noncontrast MRA provides high-quality visualization of renal arteries with no diaphragm navigator-induced artifacts, simplified setup, and shorter scan time.

Keywords

noncontrast MRA; renal MRA; online self-gating

*Correspondence to: Debiao Li, Ph.D., Cedars-Sinai Medical Center, Biomedical Imaging Research Institute, 116 N. Robertson Blvd. 800, Los Angeles, CA 90048. debiao.li@cshs.org.

INTRODUCTION

Noncontrast MR angiography (NC MRA) based on balanced steady-state free precession (bSSFP) and slab-selective inversion-recovery (IR) magnetization preparation has become an attractive alternative for imaging renal arteries (1,2) without the risk of nephrogenic systemic fibrosis (NSF) associated with gadolinium-based MR contrast agents (3,4). Besides the benefits of being contrast-free, NC MRA has additional unique advantages over its contrast-enhanced counterpart. It does not require accurate timing of the acquisition at the first-pass of contrast bolus to achieve optimal contrast and venous suppression (5). Furthermore, electrocardiograph (ECG) -triggering can be used to minimize blurring due to the aortic pulse wave (6). However the use of bSSFP three-dimensional (3D) high resolution acquisition with inversion-recovery magnetization preparation results in a relatively long scan time necessitating the usage of free-breathing approaches. Although bSSFP-based NC MRA has been proposed and developed for almost a decade (7), it has not become a routine clinical exam. One of the major hurdles has been the lack of a robust free-breathing approach to alleviate respiratory motion artifacts.

Currently, diaphragm navigator (NAV) (8) using cross-pair or 2D pencil beam is a preferred free-breathing technique. However, NAV significantly complicates exams due to its excitation volume setup, scout scans, and acceptance window setup/adjustments. Additionally, diaphragm motion only correlates to, rather than linearly represents the respiratory motion at the target slab, and the relationship between the two, defined as the “tracking-factor,” has been shown subject-specific as suggested by the work on coronary MRA (9). Another cause of NAV failure is poor signal-to-noise ratio (SNR) from the liver–lung interface in some patients (10). Based on our experience, this is due to the relatively distal location of diaphragm dome from the imaged abdominal slab causing poor field homogeneity and coil sensitivity at the liver–lung interface in some subjects, especially with wide-bore, high field [>=3 Tesla (T)] scanners. The additional cross-pair navigator excitations cause signal saturation in part of the abdominal region, which degrades the visualization of arteries in some subjects.

Respiratory gating with abdominal bellows (11) is an alternative method for free-breathing acquisition with some unique advantages. For example, the usage of bellows does not disrupt imaging sequence or interfere with magnetization preparation. However, bellows signal is not quantitative and does not vary linearly with respiratory motion at the slab being imaged (12), although it correlates with diaphragmatic and heart motion under regular breathing patterns (13). Therefore gating with bellows is not compatible with slice-tracking or retrospective motion correction. Its performance under varying breathing pattern is also problematic due to signal drift and nonlinear rescaling (14). Setup of the bellows also increases patient preparation time and prevents the use of ECG triggering in some scanners, leading to suboptimal inflow effect and aortic pulse wave-induced blurring (6).

To overcome some of these limitations, various self-gating (SG) methods have been developed that derives motion information directly from MR signal of the volume being imaged (15–17). Online self-gating is especially attractive clinically as it uses the derived motion information to guide data acquisition and/or motion correction on-the-fly therefore

does not require additional post processing or reconstruction. Recently, SG has been applied to carotid vessel wall MRI to prevent artifacts from swallowing motion (18). So far no online SG techniques have been applied in abdominal MRA to our knowledge. In this work, we developed a real-time SG technique, adaptive online self-gating (ADIOS), for free-breathing bSSFP-based renal NC MRA with adaptive scan efficiency and minimized respiratory motion artifacts. The feasibility of the new NC MRA technique was demonstrated in healthy volunteers by a comparison with the conventional NAV technique.

METHODS

Self-Gating with Inversion-Recovery Prepared bSSFP

The design of the online SG sequence is based on the clinical NC MRA protocol using inversion-recovery prepared slab-selective bSSFP. According to the central slice theorem, Fourier transform of a k-space center readout line without partition or phase encoding is the 1D projection of the entire imaging slab onto the readout direction (18). Because respiratory motion in the abdominal region has its largest displacement in the superior–inferior (SI) direction (19), an additional central k-space SG readout line in the SI direction is acquired to probe the respiratory motion at the excited slab. This SG line is embedded as an extra line at the end of each bSSFP readout block to avoid eddy current effects induced by the SI readout gradients on the following imaging data (Fig. 1a). This design also minimizes the temporal delay between SG lines and imaging data compared with using a separate SG module. Because the SG line is integrated and acquired only once per TR, the cost of SG on scanning efficiency is negligible (1 to 2%, depending on the number of segments). The field-of-view of the SG projection in the SI direction is set to the slab thickness and further cropped to its central 50% to exclude static edges introduced by the slab-selective excitation and inversion. The other acquisition parameters of the SG line are chosen identical to the imaging lines.

Adaptive Online Self-Gating

We developed a projection-based cross-correlation analysis for the online motion detection. The 1D projection of the imaging slab in the SI direction serves as the “fingerprint” of the current respiratory phase. The scan starts with a brief breath-hold at end-expiration to record the reference projection profile in the second repetition. The first repetition is not used due to the transition to steady state. In each of the subsequent repetitions, a cross-correlation coefficient (CCC) is calculated between the current projection profile and the reference profile. Respiratory motion is detected if the CCC value drops below a defined threshold and the current image lines will be rejected and reacquired in the next repetition. To compensate for signal drift and maintain scan efficiency, the threshold is automatically adjusted using a heuristic algorithm in real time. The algorithm stores the ten most recent CCC values sorted in descending order. The threshold is constantly updated to the fourth highest CCC values resulting an acceptance rate of approximately 40%. CCC outliers with abnormal low values (below mean value minus four times of standard deviation) caused by possible bulk movement are excluded from the calculation and a warning message will appear to suggest rescan (Fig. 1b). The initial threshold is set conservatively (0.998) to avoid motion in the data before the automatic algorithm starts regulating the threshold. The reference profile is unchanged throughout the acquisition to maintain the consistency of the heuristic algorithm.

Automatic Coil Combination for Reducing Static Tissue in Self-Gating

One of the drawbacks of projection-based SG is the inclusion of static tissue in the SG profile, which may lead to reduced sensitivity to detecting motion. The multicoil arrays used for parallel imaging can be used to improve respiratory motion estimation with their redundant information (20). In principle, each array coil has localized sensitivity profile, which includes different amount of static tissue leading to different levels of sensitivity to respiratory motion. Coils that are motion insensitive will compromise the performance of self-gating if a simple combination method is used, such as sum-of-square. Therefore, a coil combination method that excludes those motion-insensitive coils is necessary. Additionally, the method needs to be computationally efficient to operate in real-time for online self-gating. In this work, CCC is calculated individually from each coil with respect to its own reference and then combined into one value with a custom self-weighting function:

$$CCC_{weighted}=1-\sqrt{\sum_{allcoils}(1-CCC_i)^2}$$

where CCC_i is the CCC value calculated from the *i*th coil. In this formulation CCC values derived from motion-insensitive coils are automatically "weighted down" due to their lack of variation compared with those derived from motion-sensitive coils. As a result, the negative effects caused by static tissue are reduced for more accurate self-gating.

In Vivo Study and Self-Gating Signal Validation

Fifteen healthy volunteers (7 males, 8 females; age range, 23–51 years; mean age, 32 years) were recruited in accordance with institutional review board approval and scanned on a 3T clinical scanner (MAGNETOM Verio, Siemens AG Healthcare, Erlangen, Germany) using slab-selective inversion- recovery prepared bSSFP. Scan parameters include: ECG-triggered 41 lines/heartbeat; slab-selective inversion TI=550–750 ms; acquisition time=4–7 min depending on heart rate; TE/TR=1.9/3.8 ms; 3D transverse slab with left–right readout; field-of-view (FOV)=340 × 201 × 88 mm^2, image matrix=304 × 192 × 40, yielding acquired spatial resolution=1.1 × 1.1 × 2.2 mm^3 (interpolated to 1.1 mm isotropic); parallel imaging GRAPPA (generalized autocalibrating partially parallel acquisition)=2; bandwidth=780 Hz/pixel; flip angle=90°. For comparison, NC MRA with conventional NAV were acquired immediately before or after in a randomized manner using identical parameters and 6 mm gating window.

To validate the SG signal against the diaphragm NAV, two additional test scans were performed on three healthy volunteers in a prestudy. In the first test scan, identical FOV and other scanning parameters as previously described were used except that both NAV and SG readout were enabled in the same scan after the acquisition window during each repetition. The scan was set up for monitoring only and no gating was used. SG readout and NAV readout in each repetition have negligible temporal delay (<20 ms) for respiratory motion analysis, therefore, are considered simultaneously acquired. To evaluate the effects of slab-selective IR on SG performance, the second test scan was acquired in the same way as the first one except that no slab selective IR preparation was used.

Image Quality Evaluation and Statistics

Subjective Qualitative Scores and Maximal Vessel Length—A blinded, randomized reading was performed on images of all volunteers acquired with both free-breathing techniques by two reviewers in consensus on a workstation (Leonardo; Siemens AG Healthcare, Erlangen, Germany). Coronal and axial maximum intensity projections were performed to visualize the entire arterial tree while removing overlapping background tissues. Image quality was analyzed for three predefined segments: (i) abdominal aorta; (ii) proximal renal arteries, including main renal artery and extraparenchyma branches; (iii) distal renal arteries of intraparenchyma segmental branches. A 5-point scale was used: (i) not diagnostic (no vessel visible); (ii) poor (irregular delineation of vessel with significant blurring); (iii) acceptable (moderate artery delineation with appreciable blurring at some locations); (iv) good (good delineation with minor boundary blurring at some locations); and (v) excellent (sharp and complete vessel delineation with little or no boundary blurring). In addition, maximal visible vessel length for each kidney was measured by manual tracing from the ostium to the end of the most distal branch using the distance measurement tool on the workstation.

SNR and Contrast-to-Noise Ratio Measurements—Mean signal intensities of arterial blood (SI_{artery}) were measured in the proximal–middle portion of the left and right main renal arteries with user-specified ROIs placed within the lumen. The ROIs were randomly selected from either NAV or ADIOS image and copied over to the other image on the workstation. In case of slight translational mismatch between the NAV and ADIOS images, the ROIs were manually adjusted. Otherwise the ROIs were identical between ADIOS and NAV. Additional ROIs with area of at least 15 mm^2 were drawn within uniform areas in the medullae of right and left kidneys and signal mean (SI_{kidney}) and standard deviation (SD_{kidney}) were calculated. SD_{kidney} was used as an estimate of noise (10) because the SD of a ROI outside of body could not be used due to the inhomogeneous noise distribution with parallel imaging (21). Relative SNR and contrast-to-noise ratio (CNR) were calculated as: $rSNR=SI_{artery}/SD_{kidney}$ and $rCNR=(SI_{artery} - SI_{kidney})/SD_{kidney}$.

Vessel Sharpness—Vessel sharpness was measured using a previously published method (22). Multiplanar reformatting was performed for each 3D data set to reconstruct a 2D cross-sectional image perpendicular to the vessel axis with 1.1 mm thickness at the proximal–middle portion of each main renal artery. The locations were chosen at 2 cm distal to the renal artery ostia, same for both NAV and ADIOS images. Each 2D image was magnified (4×) by interpolation using a custom MATLAB program (ver. 2011b, The Mathworks, Natick, MA) and signal intensity profile was obtained along a user-defined line crossing the lumen center in anterior–posterior direction. On each side of the profile, the distance between the 20% and 80% points between the maximal lumen and background signal intensities were determined. The distance was averaged between both sides and the two 2D images from each 3D data set. Vessel sharpness is calculated as the reciprocal of the averaged distance.

RESULTS

Self-Gating Signal Validation

Three healthy subjects were successfully scanned with both NAV and SG readout enabled to validate SG signal against conventional NAV. The test scan with IR preparation showed apparently attenuated 1D SG projection profiles compared with the ones without IR preparation (Fig. 2a versus Fig. 2d). In both test scans, nonetheless, SG projection profiles clearly varied according to the underlying respiratory motion and SG CCC values were well matched temporally with diaphragm NAV positions (Fig. 2b,c and Fig. 2e,f). Quantitative analysis showed that the temporal correlation coefficients between SG CCC values and NAV positions was 0.76, 0.91, and 0.87 for the three subjects, respectively, with IR; while 0.82, 0.88, and 0.90 without IR (all $P<0.04$).

ADIOS Performance in Healthy Subjects

All 15 healthy volunteers completed the exam with both ADIOS and conventional NAV gating. Bulk motion was detected by ADIOS during the scan of one subject. Relative SNR, relative CNR, subjective reviewer scores of the proximal–middle arteries, and vessel sharpness measurements were tabulated in Table 1. Subjective reviewer scores of the middle–distal arteries, maximal visible vessel length measurements, and scan time information were tabulated in Table 2. A two-tailed paired t-test was performed for all measurements to determine the statistical significance of the differences between ADIOS and NAV. All measures except the *P* values were presented in the format of "mean±standard deviation" as well as "mean paired difference±standard deviation" in the tables. To control for the effects of scan time on image quality, all subjects were retrospectively sorted based on their scan time and divided into two groups: in Group A (n=9), ADIOS and NAV had similar scan time (5′37″ ±1′8″ for ADIOS versus 5′43″ ±1′6″ for NAV, $P=0.46$); in Group B (n=6), NAV used significantly longer scan time than ADIOS (mean difference between ADIOS and NAV=−2′18″ ± 52," $P=0.002$). Data from Group A, Group B, and both combined (Group T) were presented in the top, middle, and bottom four rows in the tables, respectively.

In general (Group T), satisfactory visualization of the renal arteries was achieved bilaterally except in one subject who has congenital solitary kidney (Fig. 3). ADIOS had overall higher efficiency with approximately 1 min shorter scan time on average than NAV. The reviewer scores of right middle–distal renal arteries were significantly higher with ADIOS than those with NAV ($P=0.006$). Similarly, maximal visible vessel length was found 0.35 cm longer on average in right kidneys with ADIOS than that with NAV ($P=0.012$). These improvements were mainly due to the lack of saturation with ADIOS as no significant difference was found in the left kidneys. Although rSNR, CNR, and vessel sharpness were on average better in ADIOS than NAV, statistical significance was not shown. In Group A, where the scan times of both ADIOS and NAV were similar, the performance of the two gating methods was very similar, with none of the measures significantly different. In Group B, NAV performed worse than ADIOS, although it used approximately 2 more min on average than ADIOS. ADIOS provided significantly higher vessel sharpness than NAV ($P=0.01$). ADIOS was also

superior to NAV in the maximal visible vessel length measurements and the reviewer scores of middle–distal arteries.

DISCUSSION

In this study, we have shown the feasibility of applying a real-time self-gating technique (ADIOS) to enable free-breathing renal bSSFP NC MRA without the use of diaphragm navigator (NAV) or abdominal bellows. Preliminary results of ADIOS from healthy volunteers have demonstrated similar image quality in the proximal–middle portion of renal arteries, significantly improved middle–distal vessel visualization in the right kidneys, and shorter scan time compared with conventional NAV gated acquisition.

Replacing conventional NAV with SG has several benefits for the clinical usage of abdominal NC MRA. First, it eliminates the saturation bands caused by cross-pair navigator excitation which causes signal loss in region-of-interest (e.g., renal arteries) in certain patients. Second, it no longer requires additional NAV setup and scouting, reducing the overall patient time with simplified imaging planning and less required operator expertise. In this study, the typical time needed to setup NAV was 2 to 3 min including scout scans, window adjustments, etc., and it may go up to 7 min if the NAV signal was suboptimal on the first try. Third, in contrast to NAV, SG is based on the motion information derived directly from the slab being imaged, therefore may be a better indicator of motion in situ rather than the correlated diaphragm displacement. SG signal may also have more reliable SNR than NAV signal which originates from relatively remote anatomy.

A fast automatic online gating algorithm for SG is designed in this work to minimize overall motion artifacts by trading-off between gating efficiency and residual motion within the acceptance window. It adaptively regulates the gating to compensate for respiratory signal drift and maintains a relatively defined scan time, avoiding prolonged acquisition and associated breathing pattern change and/or bulk movement. As a result of the adaptive algorithm, total scan time of ADIOS was on average 15% (59 s) shorter than that of NAV with no apparent penalty on image quality in terms of motion artifacts. In the grouped sub-analysis, NAV acquisitions that had long scan time (approximately 2 min longer than that of ADIOS on average) performed worse than ADIOS. In those cases, long scan time and its associated signal drift and/or motion were the most possible culprit for the inferior image quality with NAV. ADIOS alleviated this problem to certain extent with its adaptive gating scheme. With its adaptability ADIOS may potentially provide better image quality and diagnosis in patients who have difficulties holding still during prolonged scan.

There are limitations in the implementation of self-gating in this work. First, a short (two heartbeats) breath-hold is needed for acquiring an end-respiratory reference projection. This reference is not necessarily ideal for end-expiration phase during free-breathing because of possible mismatch between free-breathing and breath-hold even at the same respiratory phase. This limitation can be resolved in future work by using other analysis of the SG projections to extract physical translational information, such as template shifting (23), to eliminate the need for a breath-hold reference projection. Second, residual respiratory motion within the accepted data was not corrected. The main focus of this work was to

demonstrate the feasibility of a real-time SG technique to facilitate the clinical usage of NC MRA. Therefore motion correction technique that requires additional postprocessing was not used. However, in future work it is possible to incorporate motion correction techniques that are typically performed offline (24) into the online image reconstruction process.

Lastly, the online self-gating technique developed in this work is not specific to bSSFP-based renal NC MRA. It is a general free-breathing approach that can be applied for other sequences and/or other organs for respiratory motion compensation. The adaptive gating algorithm provides some flexibility for designing other SG applications. If necessary, projections in multiple directions may be used to more accurately compensate for 3D translational motion.

In conclusion, we have developed an online self-gating technique for free-breathing renal NC MRA that offers no-setup respiratory gating, shorter scan time, and improved distal vessel visualization compared with conventional diaphragm NAV.

References

1. Miyazaki M, Isoda H. Non-contrast-enhanced MR angiography of the abdomen. Eur J Radiol. 2011; 80:9–23. [PubMed: 21330081]
2. Liu X, Berg N, Sheehan J, Bi X, Weale P, Jerecic R, Carr J. Renal transplant: nonenhanced renal MR angiography with magnetization-prepared steady-state free precession. Radiology. 2009; 251:535–542. [PubMed: 19261926]
3. Marckmann P, Skov L, Rossen K, Dupont A, Damholt MB, Heaf JG, Thomsen HS. Nephrogenic systemic fibrosis: suspected causative role of gadodiamide used for contrast-enhanced magnetic resonance imaging. J Am Soc Nephrol. 2006; 17:2359–2362. [PubMed: 16885403]
4. Grobner T, Prischl F. Gadolinium and nephrogenic systemic fibrosis. Kidney Int. 2007; 72:260–264. [PubMed: 17507905]
5. Grist TM. Magnetic resonance angiography of renal artery stenosis. Am J Kidney Dis. 1994; 24:700. [PubMed: 7942831]
6. Kaandorp DW, Vasbinder GBC, de Haan MW, Kemerink GJ, van Engelshoven J. Motion of the proximal renal artery during the cardiac cycle. J Magn Reson Imaging. 2000; 12:924–928. [PubMed: 11105031]
7. Katoh M, Buecker A, Stuber M, Gunther RW, Spuentrup E. Free-breathing renal MR angiography with steady-state free-precession (SSFP) and slab-selective spin inversion: initial results. Kidney Int. 2004; 66:1272–1278. [PubMed: 15327427]
8. Liu YL, Riederer SJ, Rossman PJ, Grim RC, Debbins JP, Ehman RL. A monitoring, feedback, and triggering system for reproducible breath-hold MR imaging. Magn Reson Med. 1993; 30:507–511. [PubMed: 8255201]
9. Moghari MH, Hu P, Kissinger KV, Goddu B, Goepfert L, Ngo L, Manning WJ, Nezafat R. Subject-specific estimation of respiratory navigator tracking factor for free-breathing cardiovascular MR. Magn Reson Med. 2011; 67:1665–1672. [PubMed: 22134885]
10. Lanzman RS, Kropil P, Schmitt P, Freitag SM, Ringelstein A, Wittsack HJ, Blondin D. Nonenhanced free-breathing ECG-gated steady-state free precession 3D MR angiography of the renal arteries: comparison between 1. 5 T and 3 T. AJR Am J Roentgenol. 2010; 194:794–798. [PubMed: 20173162]
11. Ehman R, McNamara M, Pallack M, Hricak H, Higgins C. Magnetic resonance imaging with respiratory gating: techniques and advantages. AJR Am J Roentgenol. 1984; 143:1175–1182. [PubMed: 6333787]
12. Santelli C, Nezafat R, Goddu B, Manning WJ, Smink J, Kozerke S, Peters DC. Respiratory bellows revisited for motion compensation: preliminary experience for cardiovascular MR. Magn Reson Med. 2011; 65:1097–1102. [PubMed: 21413074]

13. Madore B, Farneback G, Westin CF, Durán-Mendicuti A. A new strategy for respiration compensation, applied toward 3D free-breathing cardiac MRI. Magn Reson Imaging. 2006; 24:727–737. [PubMed: 16824968]

14. Danias PG, McConnell MV, Khasgiwala VC, Chuang ML, Edelman RR, Manning WJ. Prospective navigator correction of image position for coronary MR angiography. Radiology. 1997; 203:733–736. [PubMed: 9169696]

15. Larson AC, White RD, Laub G, McVeigh ER, Li D, Simonetti OP. Self-gated cardiac cine MRI. Magn Reson Med. 2003; 51:93–102. [PubMed: 14705049]

16. Brau A, Brittain JH. Generalized self-navigated motion detection technique: preliminary investigation in abdominal imaging. Magn Reson Med. 2006; 55:263–270. [PubMed: 16408272]

17. Jin N, Lewandowski RJ, Omary RA, Larson AC. Respiratory self-gating for free-breathing abdominal phase-contrast blood flow measurements. J Magn Reson Imaging. 2009; 29:860–868. [PubMed: 19306414]

18. Fan Z, Zuehlsdorff S, Liu X, Li D. Prospective self-gating for swallowing motion: a feasibility study in carotid artery wall MRI using three-dimensional variable-flip-angle turbo spin-echo. Magn Reson Med. 2012; 67:490–498. [PubMed: 22161627]

19. Davies S, Hill A, Holmes R, Halliwell M, Jackson P. Ultrasound quantitation of respiratory organ motion in the upper abdomen. Br J Radiol. 1994; 67:1096–1102. [PubMed: 7820402]

20. Hu P, Hong S, Moghari MH, Goddu B, Goepfert L, Kissinger KV, Hauser TH, Manning WJ, Nezafat R. Motion correction using coil arrays (MOCCA) for free-breathing cardiac cine MRI. Magn Reson Med. 2011; 66:467–475. [PubMed: 21773986]

21. Dietrich O, Raya JG, Reeder SB, Reiser MF, Schoenberg SO. Measurement of signal-to-noise ratios in MR images: influence of multichannel coils, parallel imaging, and reconstruction filters. J Magn Reson Imaging. 2007; 26:375–385. [PubMed: 17622966]

22. Li D, Carr JC, Shea SM, Zheng J, Deshpande VS, Wielopolski PA, Finn JP. Coronary arteries: magnetization-prepared contrast-enhanced three-dimensional volume-targeted breath-hold MR angiography. Radiology. 2001; 219:270–277. [PubMed: 11274569]

23. Lai P, Larson AC, Bi X, Jerecic R, Li D. A dual-projection respiratory self-gating technique for whole-heart coronary MRA. J Magn Reson Imaging. 2008; 28:612–620. [PubMed: 18777542]

24. Stehning C, Bornert P, Nehrke K, Eggers H, Stuber M. Free-breathing whole-heart coronary MRA with 3D radial SSFP and self-navigated image reconstruction. Magn Reson Med. 2005; 54:476–480. [PubMed: 16032682]

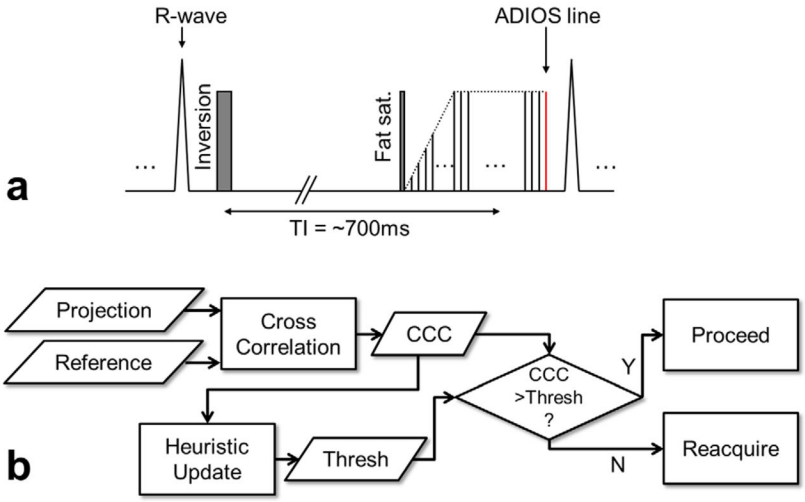

FIG. 1.

a: The pulse sequence diagram of ADIOS bSSFP NC MRA. It is based on the conventional NC MRA sequence which uses a slab-selective inversion RF pulse to suppress background tissue followed by fat-saturation, linear ramp-up catalyzing pulses, and bSSFP block. An additional alpha pulse and central k-space readout (no phase encoding) is appended at the end of each bSSFP block to acquire a self-gating line. Readout gradient is set to superior–inferior direction for maximal sensitivity to respiratory motion. **b:** The schematic diagram of the ADIOS adaptive gating algorithm used for free-breathing NC-MRA. Cross-correlation coefficient (CCC) is calculated between projection profiles and reference profile. Online gating is executed based on CCC versus the threshold. The threshold is updated in real-time using a heuristic method to maintain scan efficiency. All calculations are performed online. [Color figure can be viewed in the online issue, which is available at wileyonlinelibrary.com.]

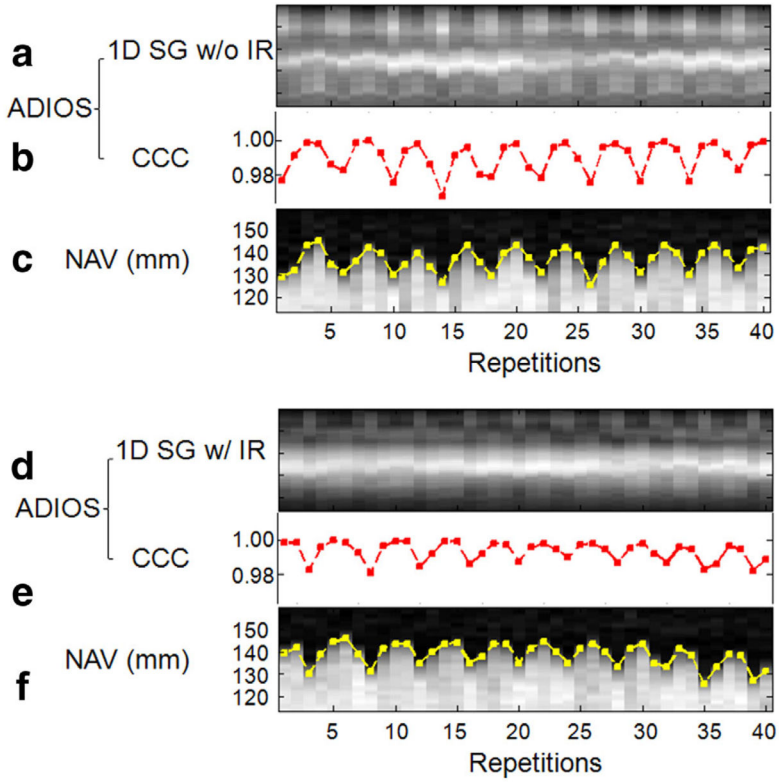

FIG. 2.

The 1D SG projection profiles without slab-selective inversion recovery (IR) (**a**) and with IR (**d**), compared with simultaneously acquired reference diaphragm navigator projections (**c,f**), all clearly showing variations due to underlying respiratory motion. CCC values (**b,e**) derived from SG projections showed high temporal correlation to the reference navigator positions (edge tracing in c,f), with temporal correlation coefficient of 0.87 with IR and 0.90 without IR (both $P<0.04$).

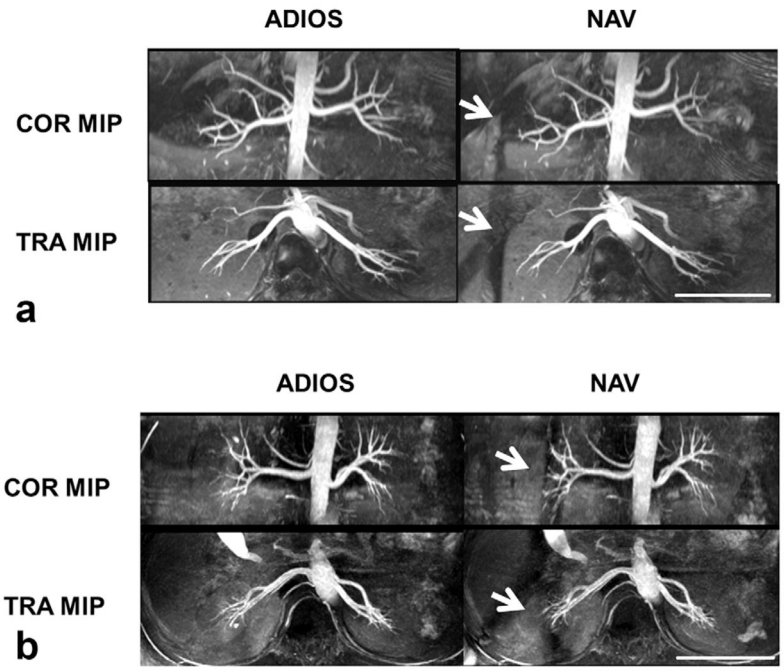

FIG. 3.

Representative coronal (COR) and transverse (TRA) maximal intensity projection (MIP) images from two healthy subjects comparing image quality of ADIOS and conventional diaphragm navigator gating (NAV), both acquired with spatial resolution of 1.1 × 1.1 × 2.2 mm^3 and TR of two heartbeats. Scale bars represent 10 cm. Note the saturation bands caused by NAV (arrows in **a,b**). In some cases, NAV saturation bands degraded the visualization of distal right renal arteries (arrows in b), whereas in the ADIOS images there was no such effect.

Table 1

Image Quality Comparison between ADIOS and NAV at Proximal–Middle Portion of Renal Arteries (Main Renal Arteries and Extraparenchyma Branches)

			Reviewer score[a]		
	rSNR	**rCNR**	**L**	**R**	**Vessel sharpness (mm^{-1})**
ADIOS (A)	44.9±6.9	31.0±6.0	4.44±0.50	4.63±0.48	0.88±0.13
NAV (A)	44.5±4.5	31.2±8.7	4.44±0.50	4.38±0.70	0.87±0.11
Paired diff.	0.4±4.2	0.1±3.6	0	0.25±0.66	0.01±0.06
P value	0.78	0.94	1	0.35	0.70
ADIOS (B)	38.3±2.9	28.1±3.7	4.33±0.75	4.50±0.76	**0.90±0.08**
NAV (B)	34.7±7.4	24.5±7.1	4.50±0.76	4.50±0.76	**0.85±0.07**
Paired diff.	3.5±4.3	3.6±4.6	−0.17±0.37	0	**0.05±0.03**
P value	0.13	0.14	0.36	1	**0.01**
ADIOS (T)	42.3±6.5	29.9±5.4	4.40±0.61	4.57±0.62	0.89±0.11
NAV (T)	40.6±9.2	28.3±6.9	4.46±0.62	4.43±0.73	0.87±0.09
Paired diff.	1.7±4.5	1.5±4.4	−0.07±0.25	0.14±0.52	0.02±0.05
P value	0.19	0.22	0.33	0.34	0.14

[a]Based on five-point scale (from 1=nondiagnostic to 5=excellent).

rSNR=relative signal-to-noise ratio; rCNR=relative contrast-to-noise ratio; ADIOS=adaptive online self-gating; NAV=diaphragm navigator; A=Group A; B=Group B; T=Total (Group T).

Table 2

Image Quality Comparison between ADIOS and NAV at Middle–Distal Portion of Renal Arteries (Intraparenchyma Branches)

	Reviewer score		MVVL (cm)		
	L	**R**	**L**	**R**	**Scan time (min's")**
ADIOS (A)	4.00±0.82	4.25±0.66	7.71±0.66	8.66±0.82	5′37″±1′8″
NAV (A)	3.89±0.87	3.88±0.93	7.91±0.61	8.34±0.58	5′43″±1′6″
Paired diff.	0.11±0.31	0.37±0.48	−0.20±0.41	0.32±0.44	−6″±23″
P value	0.35	0.080	0.20	0.092	0.46
ADIOS (B)	4.00±0.82	**3.83±0.69**	**8.07±0.82**	8.40±0.89	**5′1″±1′15″**
NAV (B)	3.83±1.07	**3.00±1.00**	**7.88±0.79**	8.01±0.10	**7′19″±1′20″**
Paired diff.	0.17±0.37	**0.83±0.69**	**0.20±0.15**	0.39±0.43	**−2′18″±52″**
P value	0.36	**0.042**	**0.034**	0.097	**0.002**
ADIOS (T)	4.00±0.82	**4.07±0.70**	7.85±0.75	**8.55±0.86**	**5′22″±1′13″**
NAV (T)	3.87±0.96	**3.50±1.05**	7.89±0.69	**8.20±0.80**	**6′21″±1′26″**
Paired diff.	0.13±0.34	**0.57±0.62**	−0.04±0.39	**0.35±0.43**	**−59″±1′15″**
P value	0.16	**0.006**	0.69	**0.012**	**0.010**

[a]Based on five-point scale (from 1=nondiagnostic to 5=excellent).

MVVL=maximal visible vessel length; ADIOS=adaptive online self-gating; NAV=diaphragm navigator; A=Group A; B=Group B; T=Total (Group T).